

Nonlinear analyses of structures with added passive devices

C. S. Tsai†

Department of Civil Engineering, Feng Chia University, Taichung, 407, Taiwan, R.O.C.

Kuei-Chi Chen‡

Graduate Institute of Civil & Hydraulic Engineering, Feng Chia University, Taichung, 407, Taiwan, R.O.C.

(Received May 14, 2002, Accepted April 9, 2004)

Abstract. Many types of passive control devices have been recognized as effective tools for improving the seismic resistance of structures. A lot of past research has been carried out to study the response of structures equipped with energy-absorbing devices by assuming that the behavior of the beam-column systems are linearly elastic. However, linear theory may not be adequate for beams and columns during severe earthquakes. This paper presents the results of research on the nonlinear responses of structures with and without added passive devices under earthquakes. A new material model based on the plasticity theory and the two-surface model for beams and columns under six components of forces is proposed to predict the nonlinear behavior of beam-column systems. And a new nonlinear beam element in consideration of shear deformation is developed to analyze the beams and columns of a structure. Numerical results reveal that linear assumption may not be appropriate for beams and columns under seismic loadings, especially for unexpectedly large earthquakes. Also, it may be necessary to adopt nonlinear beam elements in the analysis and design process to assure the safety of structures with or without the control of devices.

Key words: structural control; energy absorber; seismic resistance; nonlinear analysis.

1. Introduction

In recent years, many different passive control devices have been suggested for mitigating the harmful effects of earthquakes on structures. A lot of research in the past has also proven that energy-absorbing devices are effective tools for reducing the seismic effects on buildings. Energy-absorbing devices can be classified into velocity-dependent and velocity-independent (or displacement-dependent) devices according to their mechanical behavior (Tsai *et al.* 1998). Viscoelastic dampers (Mahmoodi 1972, Aiken *et al.* 1990, Zhang and Soong 1992, Tsai 1993, 1994, Tsai and Lee 1993, 1994) and fluid dampers (Constantinou and Symans 1993) are the most common velocity-dependent devices, but may fail to reduce structural response at the peak response

† Professor

‡ Ph. D. Student

of structure and the early stages (first few seconds) of earthquakes due to petty velocities. Velocity-independent devices, including frictional dampers (Aiken *et al.* 1988, Pall *et al.* 1991, Pekau and Guimond 1991) and metallic energy absorbers (Skinner *et al.* 1975, Kelly and Skinner 1980, Steimer and Chow 1984, Whittaker *et al.* 1989, Bergman and Hanson 1990, Tsai and Tsai 1992, 1995), may not provide any damping to the structure during minor earthquake loadings. A lot of past research and design analyzing the responses of structures equipped with passive control devices by assuming that the responses of the beam-column systems were linearly elastic has already been conducted. However, realistic behavior of beams and columns may not be maintained in elasticity during moderate or severe earthquakes. In order to predict the nonlinear behavior of structures during earthquakes as exactly as possible, the development of a more accurate model for describing the material behavior is necessary.

Any model describing plastic behavior should contain two basic features. One of these is the flow rule, which is an incremental plastic stress-strain relation. The second essential feature is the hardening rule, which defines changes of the yield surface during the change of the plastic flow as well as the change of the hardening (softening) properties of the materials. The yield surface is allowed to expand (isotropic hardening), contract (isotropic softening), translate (kinematic hardening) and distort (slip theory) in the stress space. In the past, many models have been presented for predicting the inelastic behavior of structures subjected to complex and nonproportional loading histories, such as those resulting from strong ground motions or wind gusts. Prager (1956) contended that the motion of the yield surface was in the direction of plastic strain rate and translated without rotation in the stress space. Ziegler (1959) improved this model by maintaining that the yield surface moved toward the direction of the vector connecting the center of the yield surface to the current load point. Morz (1967, 1969) introduced the notion of a field work-hardening moduli represented by a number of hypersurfaces and a new rule of kinematic hardening, which was different from those published by Prager and Ziegler. In this model, it was assumed that during translations, the individual surfaces did not intersect, but only contacted and pushed against each other consecutively. Dafalias and Popov (1975) modified Morz's model and replaced all of the surfaces with an inner yield surface and an outer limiting, or bounding surface. The motion of these two surfaces was governed by the hardening rule of Morz, and the stress-strain curves lay within two parallel straight lines XX' and YY' that provided bounds in the stress-strain space as shown in Fig. 1.

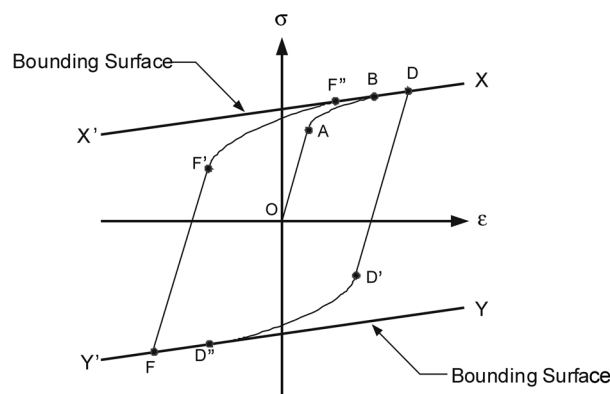


Fig. 1 Stress-strain relation in Dafalias and Popov's model

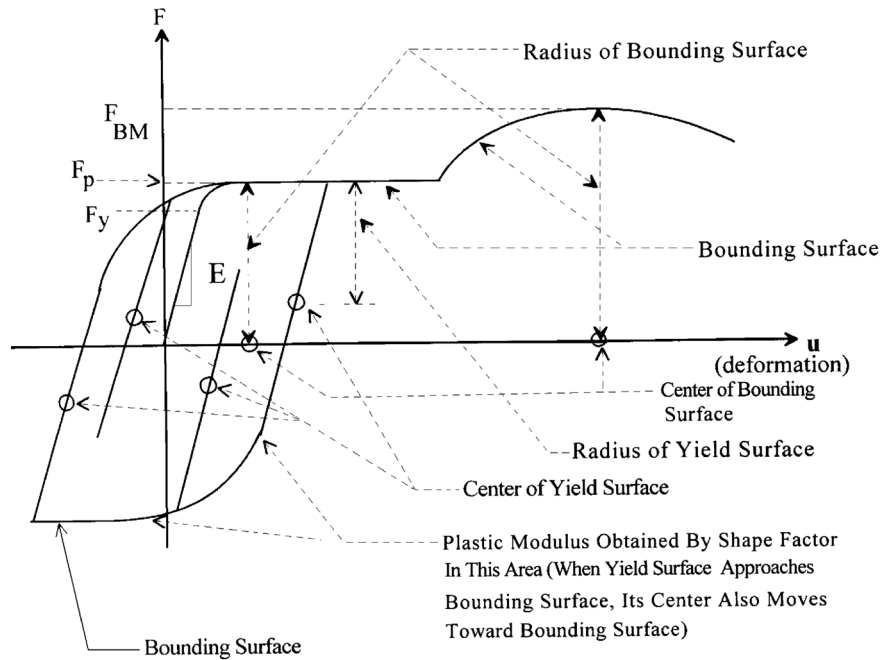


Fig. 2 Stress-strain relation in Tsai's two-surface model (Tsai 1996)

In addition, experimental results regarding the two-surface model for metals was reported by Phillips (1979). It has been observed that the bounding surface expands isotropically in the stress space and passes through the maximum stress point of the previous loading history. Also, the yield surface changes its shape and size while moving with the loading surface. The motion of the yield surface is in the direction of the stress increment or predominated by the stress increment. Tseng and Lee (1983) proposed a plastic two-surface model based on the observation of Phillips. In this model, the bounding surface expands isotropically and passes through the greatest, maximum stress state that the material has ever experienced. The yield surface, which moves within or with the bounding surface either expands for hardening materials or contracts for softening materials during the course of plastic deformation. Based on the two-surface plasticity model developed by Tseng and Lee (1983), an analytical model relating the force and strain is formulated by Yang *et al.* (1995). This model was verified through an experimental program that includes different combinations of nonproportional applied forces such as the pure bending, bending plus prescribed axial load, and the nonproportionally applied axial load and bending moment. Tsai (1996) and Tsai *et al.* (1998) indicated that to satisfy both of the monotonic and nonproportional loadings, the bounding surface should be the surface created by the monotonic loading as shown in Fig. 2.

This study modifies some aspects of the Tseng and Lee's model (1983) and proposes a generalized two-surface model consisting of six components of forces, as shown in Fig. 3. To predict the stress-strain curves during the monotonic, nonproportional, complex and cyclic loading histories, this model proposes that the bounding surface lies on the stress-strain curve caused by the monotonic loading (Tsai 1996, Tsai *et al.* 1998), as shown in Fig. 2, instead of the two parallel straight lines in Dafalias and Popov's model (1975), as shown in Fig. 1, which may not appropriately simulate both monotonic and cyclic loadings. For the convenience of computation, a

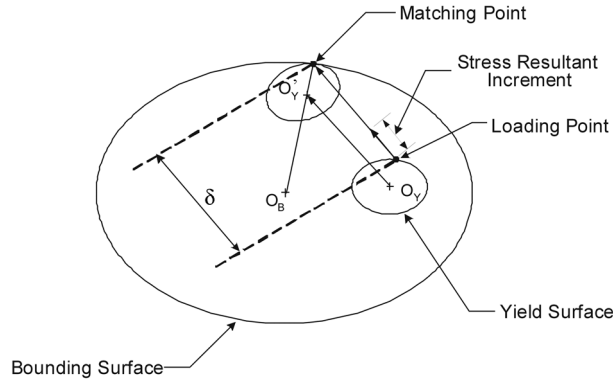


Fig. 3 Two-surface model for nonlinear plasticity

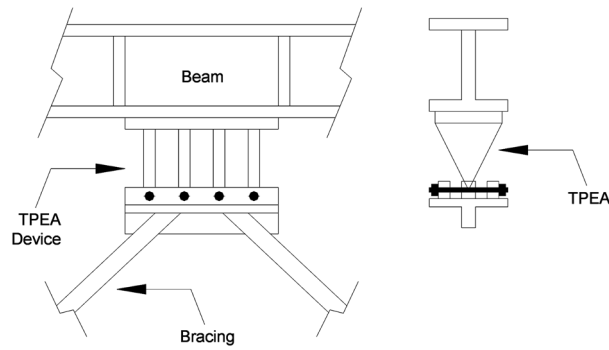


Fig. 4 Detail of TPEA device

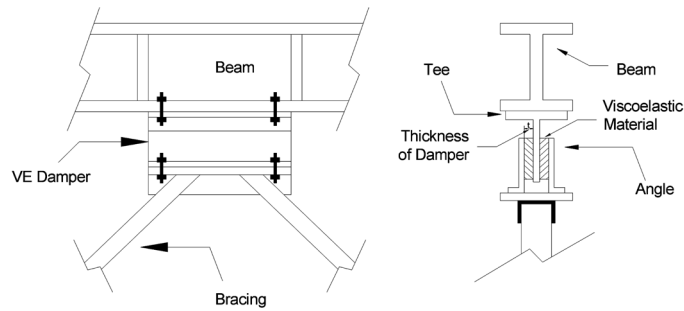


Fig. 5 Detail of VE damper

new beam element in consideration of the shear deformation is also proposed to analyze the beams and columns of structures. Details of the new model and the numerical examples of the nonlinear behavior of structures without passive devices and with TPEA devices (as shown in Fig. 4) and VE dampers (as shown in Fig. 5) are also presented in the following sections.

2. Analytical model for material nonlinearity

In order to predict the nonlinear behavior of beam elements subjected to seismic loadings accurately, a two-surface model based on the plasticity theory is proposed. This model is suitable for 2-node, 3-node, and 4-node beam elements. The theoretical derivation is briefly described below.

As shown in Fig. 3, it is assumed that the yield and bounding surfaces follow the kinematic and isotropic hardening rules, respectively. When the stress resultant (force) falls within the yield surface, the material behavior will be purely elastic. The changes of the generalized plastic modulus will be obtained by a related shape factor, while the stress resultant is located on the yield surface and moving toward the bounding surface.

In a general case, the generalized stress resultant \mathbf{F} at any section of a beam element (as shown in Fig. 6) may be written as:

$$\mathbf{F}^T = [P, V_s, V_t, M_r, M_s, M_t] \tag{1}$$

where P is the axial force and V_s, V_t are the transverse shear forces in the s - and t - directions, respectively. $M_r, M_s,$ and M_t represent torsion and bending moments about the s - and t - axes, respectively.

If ϕ is the generalized yield function for a section in the beam element, the outward, normal direction to the yield surface is given by:

$$\mathbf{n} = \frac{\phi_{,F}}{[\phi_{,F}^T \phi_{,F}]^{1/2}} \tag{2}$$

where

$$\phi_{,F}^T = \left[\frac{\partial \phi}{\partial P}, \frac{\partial \phi}{\partial V_s}, \frac{\partial \phi}{\partial V_t}, \frac{\partial \phi}{\partial M_r}, \frac{\partial \phi}{\partial M_s}, \frac{\partial \phi}{\partial M_t} \right] \tag{3}$$

\mathbf{n} is the unit outward normal vector to the yield surface.

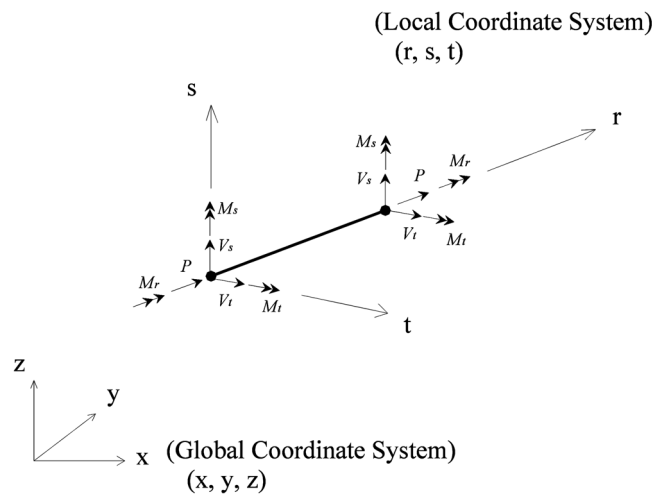


Fig. 6 Generalized stress resultants at any section of beam element

According to the normality rule, the plastic deformation increment $d\mathbf{u}_p$ is defined as:

$$d\mathbf{u}_p = \mathbf{n} du_p \quad (4)$$

where du_p is the magnitude of the plastic deformation.

The normal component of the increment of the stress resultant $d\mathbf{F}$ is defined as $d\mathbf{F}_n$ and given by:

$$d\mathbf{F}_n = \mathbf{n}(\mathbf{n}^T d\mathbf{F}) \quad (5)$$

Assuming the relationship between the stress resultant increment in the normal direction, $d\mathbf{F}_n$, and the plastic deformation, $d\mathbf{u}_p$, follows the flow rule, then one obtains

$$d\mathbf{F}_n = \mathbf{K}_p d\mathbf{u}_p \quad (6)$$

where \mathbf{K}_p is a 6×6 diagonal matrix of the generalized plastic modulus derived from the individual force-deformation relationship. If $K_p^p, K_p^{V_s}$ and $K_p^{V_t}$ represent this relationship in the axial and two transverse directions, respectively, and $K_p^{M_r}, K_p^{M_s}$ and $K_p^{M_t}$ indicate this relationship of torsion component about r -axis, and two bending components about s - and t -axes, respectively, then \mathbf{K}_p can be expressed as:

$$\begin{aligned} \mathbf{K}_p &= \text{diag}[K_p^p, K_p^{V_s}, K_p^{V_t}, K_p^{M_r}, K_p^{M_s}, K_p^{M_t}] \\ &= \text{diag}[(EA)_p, (GA_s)_p, (GA_t)_p, (GJ)_p, (EI_s)_p, (EI_t)_p] \end{aligned} \quad (7)$$

where E = elastic modulus, G = shear modulus, A = axial area, A_s = effective shear area in the s -direction, A_t = effective shear area in the t -direction, J = torsional constant, I_s = moment of inertia about the s -axis, and I_t = moment of inertia about the t -axis.

Since the projection of the tangent component of the stress resultant increment in the normal direction vanishes, one obtains

$$\mathbf{n}^T d\mathbf{F}_n = \mathbf{n}^T d\mathbf{F} \quad (8)$$

Substitution of Eqs. (4) and (6) into Eq. (8) yields

$$\mathbf{n}^T d\mathbf{F} = \mathbf{n}^T d\mathbf{F}_n = \mathbf{n}^T \mathbf{K}_p d\mathbf{u}_p = \mathbf{n}^T \mathbf{K}_p (\mathbf{n} du_p) \quad (9)$$

From Eq. (9), one can obtain:

$$du_p = \frac{\mathbf{n}^T d\mathbf{F}}{\mathbf{n}^T \mathbf{K}_p \mathbf{n}} \quad (10)$$

Substitution of Eq. (10) into Eq. (4) leads to

$$d\mathbf{u}_p = \frac{\mathbf{n} \mathbf{n}^T}{\mathbf{n}^T \mathbf{K}_p \mathbf{n}} d\mathbf{F} \quad (11)$$

If the deformation decomposition principle holds in the theory of incremental plasticity, then the total deformation, $d\mathbf{u}$, can be decomposed into the elastic part, $d\mathbf{u}_e$, and the plastic part, $d\mathbf{u}_p$. The

total deformation can be written as:

$$d\mathbf{u} = d\mathbf{u}_e + d\mathbf{u}_p \quad (12)$$

The relationship between the increments of elastic deformations and forces is given by

$$d\mathbf{F} = \mathbf{K}_e d\mathbf{u}_e \quad (13)$$

\mathbf{K}_e is a 6×6 diagonal matrix of elastic moduli (rigidities) derived from the individual force-deformation relationship.

If $K_e^P, K_e^{V_s}$ and $K_e^{V_t}$ are elastic rigidities for the axial and two transverse directions, respectively, and $K_e^{M_r}, K_e^{M_s}$ and $K_e^{M_t}$ depict elastic stiffness for the torsion and two bending components, respectively, then \mathbf{K}_e is given by

$$\begin{aligned} \mathbf{K}_e &= \text{diag}[K_e^P, K_e^{V_s}, K_e^{V_t}, K_e^{M_r}, K_e^{M_s}, K_e^{M_t}] \\ &= \text{diag}[EA, GA_s, GA_p, GJ, EI_s, EI_t] \end{aligned} \quad (14)$$

Substituting Eqs. (11) and (12) into Eq. (13), one obtains

$$\begin{aligned} d\mathbf{F} &= \mathbf{K}_e d\mathbf{u}_e = \mathbf{K}_e d\mathbf{u} - \mathbf{K}_e d\mathbf{u}_p \\ &= \mathbf{K}_e d\mathbf{u} - \mathbf{K}_e \frac{\mathbf{nn}^T}{\mathbf{n}^T \mathbf{K}_p \mathbf{n}} d\mathbf{F} \end{aligned} \quad (15)$$

Premultiplication of Eq. (15) by \mathbf{n}^T yields

$$\mathbf{n}^T d\mathbf{F} = \mathbf{n}^T \mathbf{K}_e d\mathbf{u} - \mathbf{n}^T \mathbf{K}_e \frac{\mathbf{nn}^T}{\mathbf{n}^T \mathbf{K}_p \mathbf{n}} d\mathbf{F} \quad (16)$$

Rearrangement of Eq. (16) results in

$$\mathbf{n}^T d\mathbf{F} = \frac{\mathbf{n}^T \mathbf{K}_e d\mathbf{u}}{1 + \frac{\mathbf{n}^T \mathbf{K}_e \mathbf{n}}{\mathbf{n}^T \mathbf{K}_p \mathbf{n}}} \quad (17)$$

Substitution of Eq. (17) into Eq. (15) leads to

$$\begin{aligned} d\mathbf{F} &= \mathbf{K}_e d\mathbf{u} - \mathbf{K}_e \frac{\mathbf{nn}^T \mathbf{K}_e d\mathbf{u}}{(\mathbf{n}^T \mathbf{K}_p \mathbf{n}) \left(1 + \frac{\mathbf{n}^T \mathbf{K}_e \mathbf{n}}{\mathbf{n}^T \mathbf{K}_p \mathbf{n}} \right)} \\ &= \mathbf{K}_e d\mathbf{u} - \frac{\mathbf{K}_e \mathbf{nn}^T \mathbf{K}_e}{\mathbf{n}^T \mathbf{K}_e \mathbf{n} + \mathbf{n}^T \mathbf{K}_p \mathbf{n}} d\mathbf{u} = \mathbf{K}_{ep} d\mathbf{u} \end{aligned} \quad (18)$$

where \mathbf{K}_{ep} is the modified stiffness of \mathbf{K}_e due to the plastic flow and can be expressed, with the aid of Eq. (18), as

$$\mathbf{K}_{ep} = \mathbf{K}_e - \frac{\mathbf{K}_e \mathbf{nn}^T \mathbf{K}_e}{\mathbf{n}^T \mathbf{K}_e \mathbf{n} + \mathbf{n}^T \mathbf{K}_p \mathbf{n}} \quad (19)$$

Assume that the yield function ϕ for the beam section is given by:

$$C_1(p - \alpha_p)^2 + C_2(m_t - \alpha_{mt})^2 + C_3(m_s - \alpha_{ms})^2 + C_4(p - \alpha_p)^2(m_t - \alpha_{mt})^2 + C_5(p - \alpha_p)^2(m_s - \alpha_{ms})^2 + C_6(m_t - \alpha_{mt})^2(m_s - \alpha_{ms})^2 + C_7(v_s - \alpha_{vs})^2 + C_8(v_t - \alpha_{vt})^2 + C_9(m_r - \alpha_{mr})^2 = 1.0 \quad (20)$$

where

$$p = \frac{P}{P_p}, \quad m_t = \frac{M_t}{M_{pt}}, \quad m_s = \frac{M_s}{M_{ps}}, \quad m_r = \frac{M_r}{M_{pr}}, \quad v_s = \frac{V_s}{V_{ps}}, \quad \text{and} \quad v_t = \frac{V_t}{V_{pt}} \quad (21)$$

P is the axial force; V_s is the shear force in the s -direction; V_t is the shear force in the t -direction; M_r is the torsion about the r -axis; M_s is the bending moment about the s -axis; and M_t is the bending moment about the t -direction. P_p = the axial force in the r -direction to result in the beam element yield in the entire section, V_{ps} and V_{pt} = the transverse shear forces in the s - and t -directions to result in the beam element yield in the entire section, respectively; M_{pr} , M_{ps} , and M_{pt} = torsion and bending moments about the r -, s - and the t - directions to cause the beam element yield in the entire section, respectively.

If one defines $N = [\phi_{,F} \ \phi_{,F}]^{1/2}$, then the unit normal direction, \mathbf{n} , is given as

$$\begin{aligned} \mathbf{n} &= [n_1, n_2, n_3, n_4, n_5, n_6]^T \\ &= \frac{1}{N} \left[\frac{\partial \phi}{\partial P}, \frac{\partial \phi}{\partial V_s}, \frac{\partial \phi}{\partial V_t}, \frac{\partial \phi}{\partial M_r}, \frac{\partial \phi}{\partial M_s}, \frac{\partial \phi}{\partial M_t} \right]^T \end{aligned} \quad (22)$$

Let $S = \mathbf{n}^T \mathbf{K}_e \mathbf{n} + \mathbf{n}^T \mathbf{K}_p \mathbf{n}$, then

$$S = n_1^2 |K_e^P + K_p^P| + n_2^2 |K_e^{V_s} + K_p^{V_s}| + n_3^2 |K_e^{V_t} + K_p^{V_t}| + n_4^2 |K_e^{M_r} + K_p^{M_r}| + n_5^2 |K_e^{M_s} + K_p^{M_s}| + n_6^2 |K_e^{M_t} + K_p^{M_t}| \quad (23)$$

With the aid of Eqs. (7), (14), (19) and (23), the \mathbf{K}_{ep} of Eq. (19) can be derived as the following matrix form:

$$\mathbf{K}_{ep} = \begin{bmatrix} K_e^P - \frac{n_1^2 (K_e^P)^2}{S} & -\frac{n_1 n_2 K_e^P K_e^{V_s}}{S} & -\frac{n_1 n_3 K_e^P K_e^{V_t}}{S} & -\frac{n_1 n_4 K_e^P K_e^{M_r}}{S} & -\frac{n_1 n_5 K_e^P K_e^{M_s}}{S} & -\frac{n_1 n_6 K_e^P K_e^{M_t}}{S} \\ & K_e^{V_s} - \frac{n_2^2 (K_e^{V_s})^2}{S} & -\frac{n_2 n_3 K_e^{V_s} K_e^{V_t}}{S} & -\frac{n_2 n_4 K_e^{V_s} K_e^{M_r}}{S} & -\frac{n_2 n_5 K_e^{V_s} K_e^{M_s}}{S} & -\frac{n_2 n_6 K_e^{V_s} K_e^{M_t}}{S} \\ & & K_e^{V_t} - \frac{n_3^2 (K_e^{V_t})^2}{S} & -\frac{n_3 n_4 K_e^{V_t} K_e^{M_r}}{S} & -\frac{n_3 n_5 K_e^{V_t} K_e^{M_s}}{S} & -\frac{n_3 n_6 K_e^{V_t} K_e^{M_t}}{S} \\ & & & K_e^{M_r} - \frac{n_4^2 (K_e^{M_r})^2}{S} & -\frac{n_4 n_5 K_e^{M_r} K_e^{M_s}}{S} & -\frac{n_4 n_6 K_e^{M_r} K_e^{M_t}}{S} \\ & & & & K_e^{M_s} - \frac{n_5^2 (K_e^{M_s})^2}{S} & -\frac{n_5 n_6 K_e^{M_s} K_e^{M_t}}{S} \\ & & & & & K_e^{M_t} - \frac{n_6^2 (K_e^{M_t})^2}{S} \end{bmatrix} \quad (24)$$

SYMMETRIC

From the geometrical relationship, the distance δ between the loading point at the yield surface and the matching point at the bounding surface, as shown in Fig. 3, is given by

$$\delta = \frac{-(F_i \dot{F}_i) + \sqrt{(F_i \dot{F}_i)^2 - (\dot{F}_i \dot{F}_i)(F_i F_i - F_B^2)}}{\sqrt{\dot{F}_i \dot{F}_i}}, \quad i = 1 \sim 6 \quad (25)$$

where $F_1 = \frac{P}{P_p}$, $F_2 = \frac{V_s}{V_{ps}}$, $F_3 = \frac{V_t}{V_{pt}}$, $F_4 = \frac{M_r}{M_{pr}}$, $F_5 = \frac{M_s}{M_{ps}}$, $F_6 = \frac{M_t}{M_{pt}}$, $\dot{F}_1 = \frac{dP}{P_p}$, $\dot{F}_2 = \frac{dV_s}{V_{ps}}$, $\dot{F}_3 = \frac{dV_t}{V_{pt}}$, $\dot{F}_4 = \frac{dM_r}{M_{pr}}$, $\dot{F}_5 = \frac{dM_s}{M_{ps}}$, $\dot{F}_6 = \frac{dM_t}{M_{pt}}$ and $F_B =$ yield force of the bounding surface. While the stress resultant is on the yield surface and approaching the bounding surface, the generalized plastic moduli K_p^P , $K_p^{V_s}$, $K_p^{V_t}$, $K_p^{M_r}$, $K_p^{M_s}$ and $K_p^{M_t}$ may be obtained by the following equations:

$$K_p^P = \left(1 + h_1 \frac{\delta}{\delta_{ini} - \delta}\right) (K_0)_p^P \quad (26)$$

$$K_p^{V_s} = \left(1 + h_2 \frac{\delta}{\delta_{ini} - \delta}\right) (K_0)_p^{V_s} \quad (27)$$

$$K_p^{V_t} = \left(1 + h_3 \frac{\delta}{\delta_{ini} - \delta}\right) (K_0)_p^{V_t} \quad (28)$$

$$K_p^{M_r} = \left(1 + h_4 \frac{\delta}{\delta_{ini} - \delta}\right) (K_0)_p^{M_r} \quad (29)$$

$$K_p^{M_s} = \left(1 + h_5 \frac{\delta}{\delta_{ini} - \delta}\right) (K_0)_p^{M_s} \quad (30)$$

$$K_p^{M_t} = \left(1 + h_6 \frac{\delta}{\delta_{ini} - \delta}\right) (K_0)_p^{M_t} \quad (31)$$

where

$$h_i = \frac{A_i}{\delta_{ini}^2}, \quad i = 1 \sim 6 \quad (32)$$

δ_{ini} = the distance between the loading and matching points while the material starts yielding; $(K_0)_p^P$, $(K_0)_p^{V_s}$, $(K_0)_p^{V_t}$, $(K_0)_p^{M_r}$, $(K_0)_p^{M_s}$ and $(K_0)_p^{M_t}$ = generalized plastic moduli associated with the bounding surface; A_1 , A_2 , A_3 , A_4 , A_5 and A_6 are unknown coefficients related to shape factors to be determined from the experimental results by applying the curve fitting method. It should be noted that the ranges of shape factors h_1 , h_2 , h_3 , h_4 , h_5 and h_6 can also be acquired from the experimental data.

Knowledge of the yield surface's motion is essential for the determination of δ , δ_{ini} , and the generalized plastic modulus. The following is the derivation of the motion of the yield surface. According to the experimental observations (Phillips and Lee 1979), the yield surface moves along the direction of the stress resultant increment.

As shown in Fig. 3, the center of the yield surface moves from O_Y to $O_{Y'}$ in the force space; whereas, the stress resultant moves from the loading point to the matching point. If l_i is a component of the unit vector of the stress resultant increment, then the component of the unit vector, v_i , along the direction $\overrightarrow{O_Y O_{Y'}}$ can be readily obtained from trigonometry; that is,

$$v_i = \frac{1}{L} \left[\frac{(F_B - F_Y)(F_i + \delta l_i)}{[(F_j + \delta l_j)(F_j + \delta l_j)]^{1/2}} - \alpha_i \right], \quad i = 1 \sim 6 \quad (33)$$

where L = the distance between the points O_Y and $O_{Y'}$; α_i = the coordinate of the center of the yield surface in the force space, and F_B and F_Y are the yield stresses of the bounding and yield surfaces, respectively. If $d\alpha_i$ is defined as the motion of the center of the yield surface, then with the aid of the consistency rule and Eq. (33), the following equations can be obtained:

$$|d\alpha| = \frac{A(dP/P_p) + B(dV_s/V_{ps}) + C(dV_t/V_{pt}) + D(dM_r/M_{pr}) + E(dM_s/M_{ps}) + F(dM_t/M_{pt})}{Av_1 + Bv_2 + Cv_3 + Dv_4 + Ev_5 + Fv_6} \quad (34)$$

and

$$d\alpha_i = |d\alpha| v_i, \quad i = 1 \sim 6 \quad (35)$$

where

$$A = \frac{\partial \phi}{\partial P}, \quad B = \frac{\partial \phi}{\partial V_s}, \quad C = \frac{\partial \phi}{\partial V_t}, \quad D = \frac{\partial \phi}{\partial M_r}, \quad E = \frac{\partial \phi}{\partial M_s}, \quad \text{and} \quad F = \frac{\partial \phi}{\partial M_t} \quad (36)$$

3. Finite element formulation for beam element

Taking the shear deformation effect into consideration, a nonlinear finite element formulation for a beam with four nodes is presented in this section. The same derivation procedures are applicable to the 2-node and 3-node beam elements. In these formulations, six degrees of freedom in the global coordinate system x , y and z , and six degrees of freedom in the local coordinate system r , s and t for each node are depicted in Fig. 7.

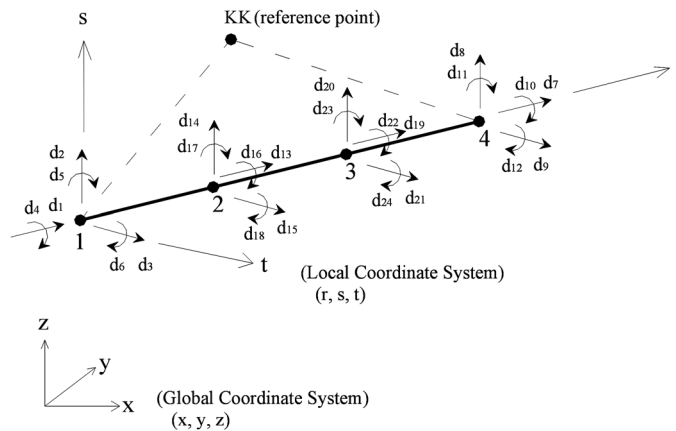


Fig. 7 General 4-node beam element

If v and θ_t denote the displacement in the s -direction and the rotation about the t -axis, then the displacement and rotation distributions along the r -direction can be expressed as:

$$v = N_1 d_2 + N_2 d_8 + N_3 d_{14} + N_4 d_{20} \quad (37)$$

$$\theta_t = N_1 d_6 + N_2 d_{12} + N_3 d_{18} + N_4 d_{24} \quad (38)$$

where N_i is the shape function and d_j is the j _{th} degree of freedom. If a cubic interpolation function is adopted along the r -axis, the shape functions can be expressed as:

$$N_1 = \frac{-4.5}{L^3} \left(r - \frac{L}{3} \right) \left(r - \frac{2L}{3} \right) (r - L) \quad (39)$$

$$N_2 = \frac{4.5}{L^3} r \left(r - \frac{L}{3} \right) \left(r - \frac{2L}{3} \right) \quad (40)$$

$$N_3 = \frac{13.5}{L^3} r \left(r - \frac{2L}{3} \right) (r - L) \quad (41)$$

$$N_4 = \frac{-13.5}{L^3} r \left(r - \frac{L}{3} \right) (r - L) \quad (42)$$

where L is the length of the beam element.

The bending curvature about the t -axis, ϕ_t , is given by:

$$\begin{aligned} \phi_t &= \frac{\partial \theta_t}{\partial r} = \frac{dN_1}{dr} d_6 + \frac{dN_2}{dr} d_{12} + \frac{dN_3}{dr} d_{18} + \frac{dN_4}{dr} d_{24} \\ &= \mathbf{B}_t \mathbf{D}_t \end{aligned} \quad (43)$$

where

$$\mathbf{B}_t = \left[\frac{dN_1}{dr} \quad \frac{dN_2}{dr} \quad \frac{dN_3}{dr} \quad \frac{dN_4}{dr} \right] \quad (44)$$

$$\mathbf{D}_t = [d_6, d_{12}, d_{18}, d_{24}]^T \quad (45)$$

With the same procedure as described earlier, the bending curvature about the s -axis, ϕ_s , is obtained:

$$\begin{aligned} \phi_s &= -\frac{dN_1}{dr} d_5 - \frac{dN_2}{dr} d_{11} - \frac{dN_3}{dr} d_{17} - \frac{dN_4}{dr} d_{23} \\ &= \mathbf{B}_s \mathbf{D}_s \end{aligned} \quad (46)$$

where

$$\mathbf{B}_s = \left[-\frac{dN_1}{dr} \quad -\frac{dN_2}{dr} \quad -\frac{dN_3}{dr} \quad -\frac{dN_4}{dr} \right] \quad (47)$$

$$\mathbf{D}_s = [d_5, d_{11}, d_{17}, d_{23}]^T \quad (48)$$

The displacement in the axial direction (r -axis), u , can be expressed as:

$$u = N_1 d_1 + N_2 d_7 + N_3 d_{13} + N_4 d_{19} \quad (49)$$

The axial strain, ε_r , is obtained as:

$$\begin{aligned} \varepsilon_r &= \frac{\partial u}{\partial r} = \frac{\partial N_1}{\partial r} d_1 + \frac{\partial N_2}{\partial r} d_7 + \frac{\partial N_3}{\partial r} d_{13} + \frac{\partial N_4}{\partial r} d_{19} \\ &= \mathbf{B}_r \mathbf{D}_r \end{aligned} \quad (50)$$

where

$$\mathbf{B}_r = \left[\frac{\partial N_1}{\partial r} \quad \frac{\partial N_2}{\partial r} \quad \frac{\partial N_3}{\partial r} \quad \frac{\partial N_4}{\partial r} \right] \quad (51)$$

$$\mathbf{D}_r = [d_1, d_7, d_{13}, d_{19}]^T \quad (52)$$

If ϕ_r represents the torsion curvature, the following formula can be acquired by assuming a quadratic variation and complying with the previous procedures.

$$\begin{aligned} \phi_r &= \frac{\partial \theta_{Torsion}}{\partial r} = \frac{\partial N_1}{\partial r} d_4 + \frac{\partial N_2}{\partial r} d_{10} + \frac{\partial N_3}{\partial r} d_{16} + \frac{\partial N_4}{\partial r} d_{22} \\ &= \mathbf{B}_{Torsion} \mathbf{D}_{Torsion} \end{aligned} \quad (53)$$

where

$$\mathbf{B}_{Torsion} = \left[\frac{\partial N_1}{\partial r} \quad \frac{\partial N_2}{\partial r} \quad \frac{\partial N_3}{\partial r} \quad \frac{\partial N_4}{\partial r} \right] \quad (54)$$

$$\mathbf{D}_{Torsion} = [d_4, d_{10}, d_{16}, d_{22}]^T \quad (55)$$

If γ_s represents the shear deformation in the s -direction, it can be obtained as:

$$\begin{aligned} \gamma_s &= -\left(\theta_t - \frac{\partial v}{\partial r} \right) = \frac{\partial N_1}{\partial r} d_2 + \frac{\partial N_2}{\partial r} d_8 + \frac{\partial N_3}{\partial r} d_{14} + \frac{\partial N_4}{\partial r} d_{20} - N_1 d_6 - N_2 d_{12} - N_3 d_{18} - N_4 d_{24} \\ &= \mathbf{B}_{rs} \mathbf{D}_{rs} \end{aligned} \quad (56)$$

where

$$\mathbf{B}_{rs} = \left[\frac{dN_1}{dr} \quad \frac{dN_2}{dr} \quad \frac{dN_3}{dr} \quad \frac{dN_4}{dr} \quad -N_1 \quad -N_2 \quad -N_3 \quad -N_4 \right] \quad (57)$$

$$\mathbf{D}_{rs} = [d_2, d_8, d_{14}, d_{20}, d_6, d_{12}, d_{18}, d_{24}]^T \quad (58)$$

If w denotes the displacement in the t -direction, the shear deformation in the t -direction, γ_t , can be

obtained as:

$$\begin{aligned} \gamma_t = -\left(\theta_s - \frac{\partial w}{\partial r}\right) &= \frac{\partial N_1}{\partial r} d_3 + \frac{\partial N_2}{\partial r} d_9 + \frac{\partial N_3}{\partial r} d_{15} + \frac{\partial N_4}{\partial r} d_{21} - N_1 d_5 - N_2 d_{11} - N_3 d_{17} - N_4 d_{23} \\ &= \mathbf{B}_{rt} \mathbf{D}_{rt} \end{aligned} \quad (59)$$

where

$$\mathbf{B}_{rt} = \left[\frac{dN_1}{dr} \quad \frac{dN_2}{dr} \quad \frac{dN_3}{dr} \quad \frac{dN_4}{dr} \quad -N_1 \quad -N_2 \quad -N_3 \quad -N_4 \right] \quad (60)$$

$$\mathbf{D}_{rt} = [d_3, d_9, d_{15}, d_{21}, d_5, d_{11}, d_{17}, d_{23}]^T \quad (61)$$

By virtue of the virtual work, the stiffness matrix \mathbf{K}_{local} for the beam element in the local coordinate system can be obtained as:

$$\mathbf{K}_{local} = \int_0^L \mathbf{B}^T \mathbf{K}_{ep} \mathbf{B} dr \quad (62)$$

where \mathbf{B} is a 6×24 matrix assembled from the matrices \mathbf{B}_r , \mathbf{B}_s , \mathbf{B}_t , \mathbf{B}_{rs} , \mathbf{B}_{rt} , and $\mathbf{B}_{Torsion}$ and given by:

$$\mathbf{B} = [\mathbf{B}_r, \mathbf{B}_{rs}, \mathbf{B}_{rt}, \mathbf{B}_{Torsion}, \mathbf{B}_s, \mathbf{B}_t]^T \quad (63)$$

Applying the matrix transformation, the global stiffness \mathbf{K}_{global} , a 24×24 matrix for a beam element, is given by:

$$\mathbf{K}_{global} = \mathbf{R}^T \mathbf{K}_{local} \mathbf{R} \quad (64)$$

where \mathbf{R} is a transformation matrix associated with the local and global coordinate systems.

4. Properties of structures and dampers

This study considers a building with flexible ductile moment resisting frames in order to examine the realistic behavior of the structure mounted with TPEA devices, viscoelastic dampers, and without dampers from minor earthquakes to severe ground motions. As shown in Fig. 8, a 10-story building is given as an example to present the proposed concept. The elastic modulus and Poisson's ratio are 0.207×10^{12} N/m² and 0.3, respectively. The yield stress is 250×10^6 N/m² for beams and columns. The weight of each floor is 13.38 KN/m. In the analysis, it is assumed that each floor is rigid in its own plan. The yield function for beams and columns is $\phi = (p - \alpha_p)^2 + (m_t - \alpha_{mt})^2 = 1.0$.

As shown in Figs. 4, 5 and 9, TPEA devices and VE dampers are chosen to install at each story by chevron braces, respectively. The analytic model of TPEA devices proposed by Tsai and Tsai (1995) and the analytic model of VE dampers proposed by Tsai and Lee (1994) are adopted in the analysis. The design methods of the structure equipped with TPEA devices and VE dampers refer to the parametric studies reported in Pong *et al.* (1994). The geometrical properties of the TPEA element are listed in Table 1, where N = number of the tapered plate; T = plate thickness;

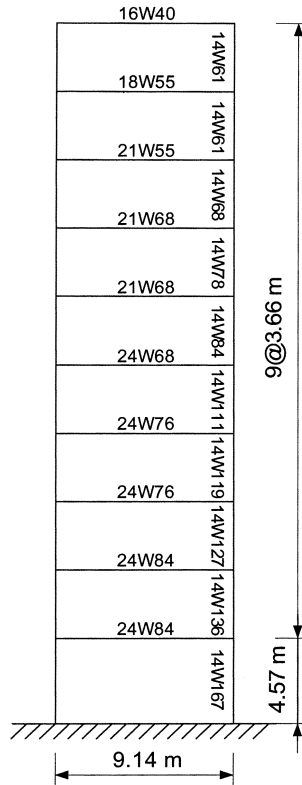


Fig. 8 Ten-story building

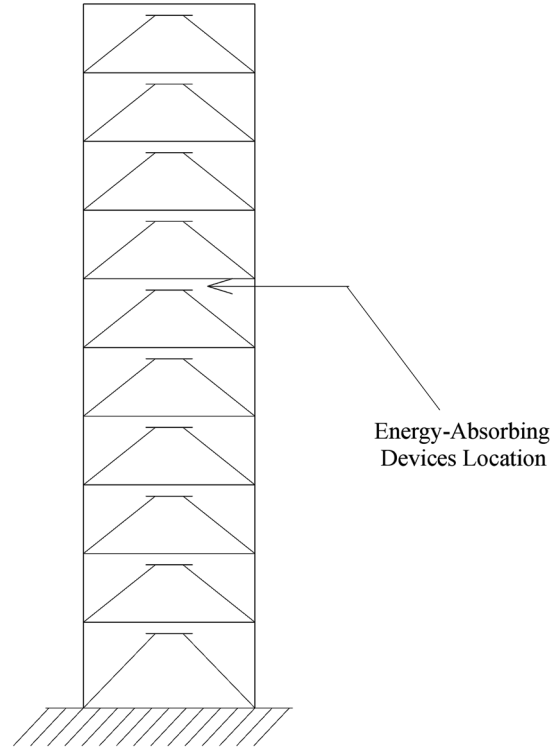


Fig. 9 Ten-story building equipped with energy-absorbing devices

B and h = base width and height of the tapered plate, respectively. The yield stress for steel plates in the TPEA devices is $295.8 \times 10^6 \text{ N/m}^2$. The geometrical properties of VE dampers are given in Table 2, where t = thickness of layers of VE damper; Area = the cross-section area of VE damper.

The response of the structure with and without dampers was compared when the structure was subjected to different peak ground accelerations from 0.1 g to 1.0 g of the El Centro earthquake (1940 Imperial Valley Earthquake, El Centro record, Component NS). In this investigation, two kinds of beam-column systems are presented in the analysis. One is the linear beam-column system, which adopts linear beam elements for the beams and columns of the structure. The other is the nonlinear beam-column system, which adopts the nonlinear beam elements proposed in this study for the beams and columns of the structure. The selected response parameters include: (1) the roof displacement, which is the lateral displacement at the top relative to the ground; (2) the moment-curvature relationship at 5th story beam-end, where plastic hinge occurred earlier than most of other structural members; (3) the hysteresis loops of the passive device on the fifth story. We also identify whether yielding of structural members occurs by observing force-displacement relationship at every integration point of the nonlinear beam-column system. Besides, if the stresses of beams and columns are beyond the elastic limit, the results will be different between the linear and nonlinear beam-column systems. The finite element formulations for the nonlinear beam, the TPEA, and viscoelastic dampers are installed in the NSAT computer program (Tsai 1996).

Table 1 Properties of TPEA devices

Floor	B (cm)	T (cm)	h (cm)	N
1	11.32	2	13.97	5
2	9.09	2	13.97	5
3	8.08	2	13.97	5
4	9.23	2	13.97	4
5	8.40	2	13.97	4
6	9.26	2	13.97	3
7	10.77	2	15.24	3
8	9.31	2	15.24	3
9	7.82	2	15.24	3
10	7.46	2	15.24	3

Table 2 Properties of VE dampers

Floor	t (cm)	Area (cm ²)
1	2.54	1354.84
2	2.54	812.90
3	2.54	812.90
4	2.54	812.90
5	2.54	812.90
6	2.54	812.90
7	2.54	812.90
8	2.54	812.90
9	2.54	812.90
10	2.54	812.90

5. Numerical results

The calculated natural frequency of the modal structure, as shown in Fig. 8, without added dampers corresponding to the first mode of vibration is 0.733 Hz. The first modal frequencies of the structure with TPEA devices and viscoelastic dampers are 1.176 Hz and 1.155 Hz, respectively.

Table 3 gives the maximum roof displacements of the structure with and without energy-dissipation devices under different levels of the El Centro earthquake ground motions. With the aid of observing force-displacement relationship at every integration point of the nonlinear beam element, it can be determined that the structure without dampers started yielding at about 0.3 g PGA; the main structure of the building with added TPEA devices started yielding at about 0.8 g PGA; the main structure of the building with added viscoelastic dampers started yielding at about 0.6 g PGA. Fig. 10 depicts the roof displacement envelopes at top of the structures with and without dampers subjected to different earthquake peak acceleration from 0.1 g to 1.0 g of the El Centro earthquake ground motion. It can be seen that additional energy absorbers can effectively reduce structural response during earthquake excitations. This figure also shows that once yielding occurs, parts of main structural members offer hysteresis damping to dissipate seismic energy.

Table 3 Comparisons of maximum roof displacements with and without dampers under scaled El Centro earthquakes

PGA (g)	Maximum Roof Displacement (mm)					
	Linear Beam-Column System	Nonlinear Beam-Column System	Linear Beam-Column System + TPEAs	Nonlinear Beam-Column System + TPEAs	Linear Beam-Column System + VE Dampers	Nonlinear Beam-Column System + VE Dampers
0.1	67.29	67.29	46.30	46.30	41.78	41.78
0.2	134.58	134.58	70.77	70.77	84.24	84.24
0.3	201.87	201.85	97.03	97.03	127.89	127.89
0.4	269.16	239.01	129.18	129.18	173.01	173.01
0.5	336.45	262.78	162.78	162.78	219.54	219.54
0.6	403.74	270.91	198.56	198.56	267.24	267.12
0.7	471.03	308.09	235.43	235.43	315.68	313.54
0.8	538.32	352.39	272.95	273.13	364.39	350.92
0.9	605.61	397.42	310.62	309.77	412.97	374.04
1.0	672.90	442.41	349.27	338.47	461.08	411.19

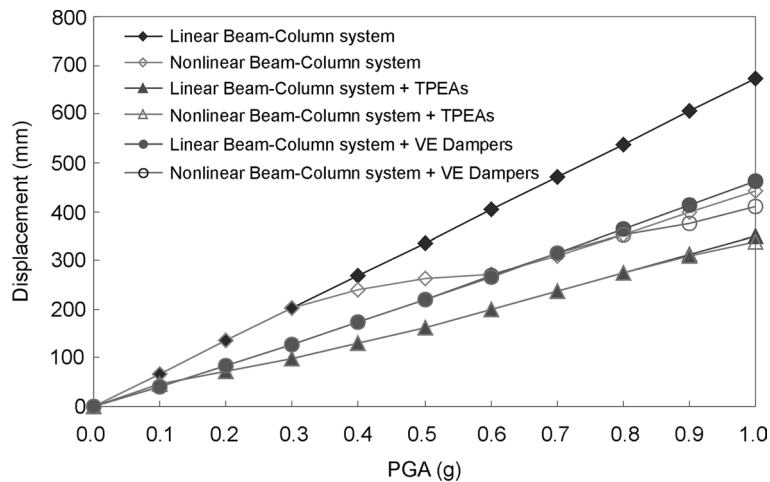


Fig. 10 Roof displacement envelopes with and without dampers under different levels of El Centro earthquake

The comparison of the time-history response of the roof displacement for the bare structure subjected to the El Centro earthquake of 0.6 g PGA is shown in Fig. 11. The comparison of the roof displacement for the structure equipped with TPEA devices and subjected to the El Centro earthquake of 0.9 g PGA is shown in Fig. 12. The comparison of the roof displacement for the structure equipped with viscoelastic dampers and subjected to the El Centro earthquake of 0.8 g PGA is shown in Fig. 13. These figures show that the roof displacements of the linear and nonlinear beam-column systems are distinguishable while the main structure is yielding. The moment-curvature relationship at the fifth story beam-end for the bare structure subjected to the El Centro earthquake of 0.6 g PGA is shown in Fig. 14. The moment-curvature relationship at the fifth story

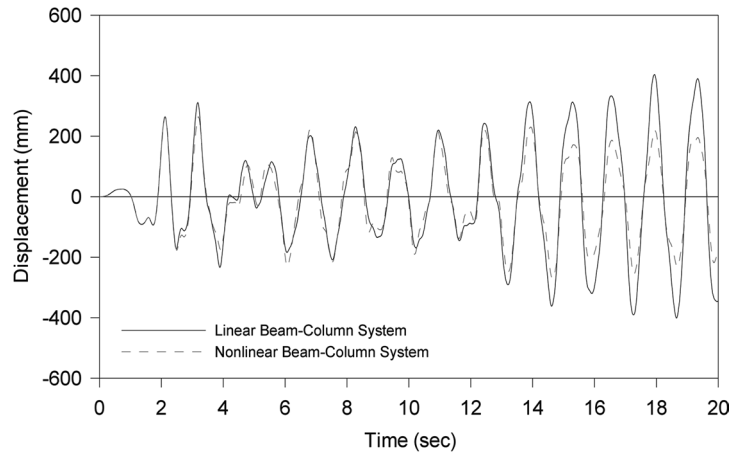


Fig. 11 Comparison of roof displacement while bare structure is subjected to 0.6 g El Centro earthquake

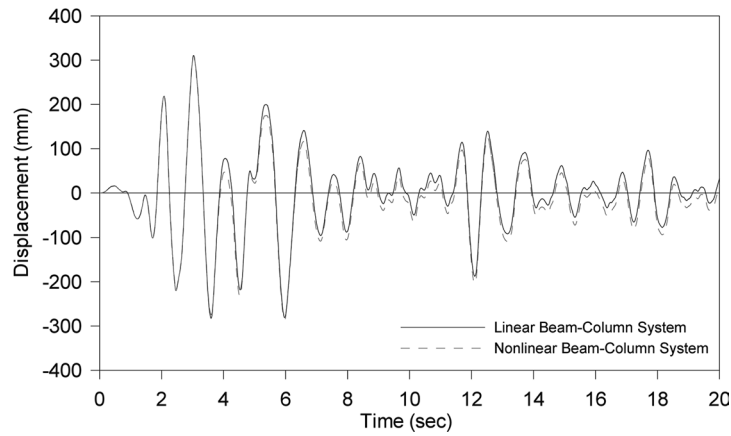


Fig. 12 Comparison of roof displacement for structure equipped with TPEA devices is subjected to 0.9 g El Centro earthquake

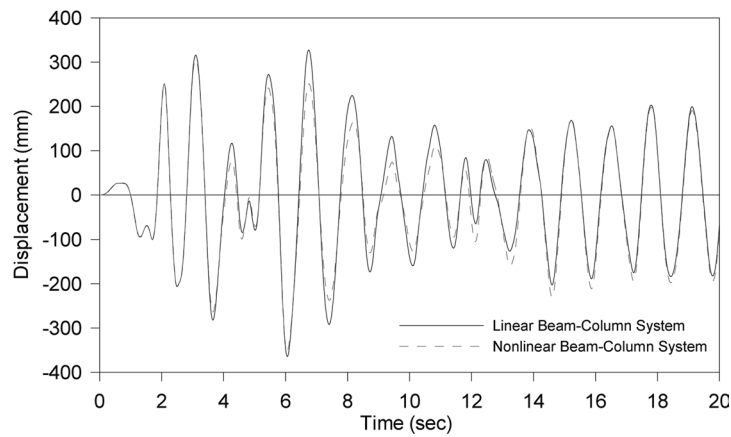


Fig. 13 Comparison of roof displacement for structure equipped with viscoelastic dampers is subjected to 0.8 g El Centro earthquake

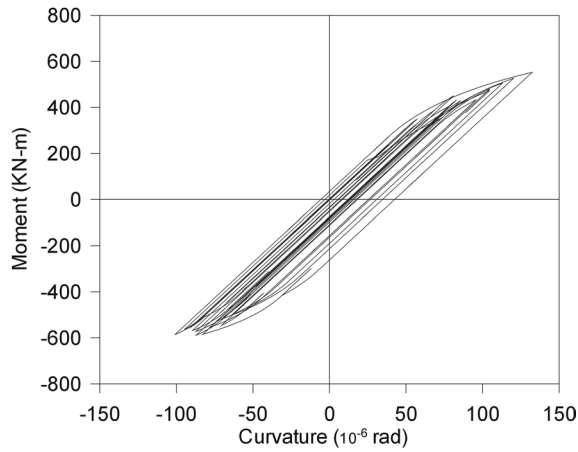


Fig. 14 Moment-curvature relationship at fifth story beam-end of bare structure under 0.6 g El Centro earthquake

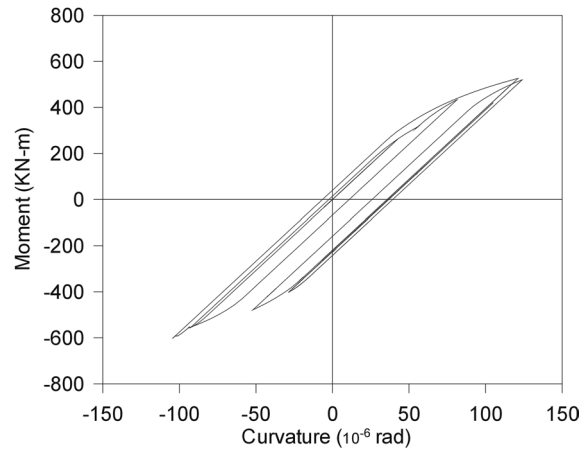


Fig. 15 Moment-curvature relationship at fifth story beam-end of structure equipped with TPEA devices under 0.9 g El Centro Earthquake

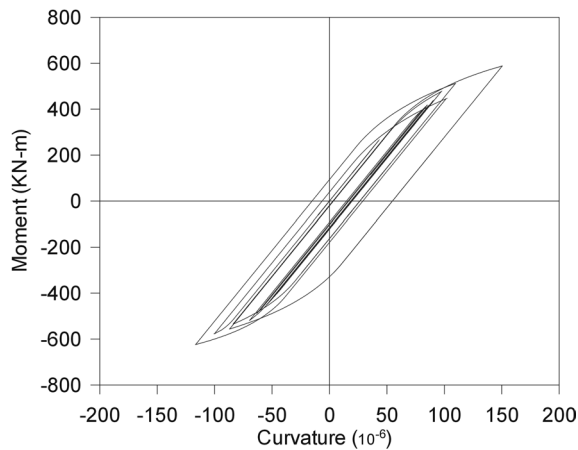


Fig. 16 Moment-curvature relationship at fifth story beam-end of structure equipped with viscoelastic dampers under 0.8 g El Centro earthquake

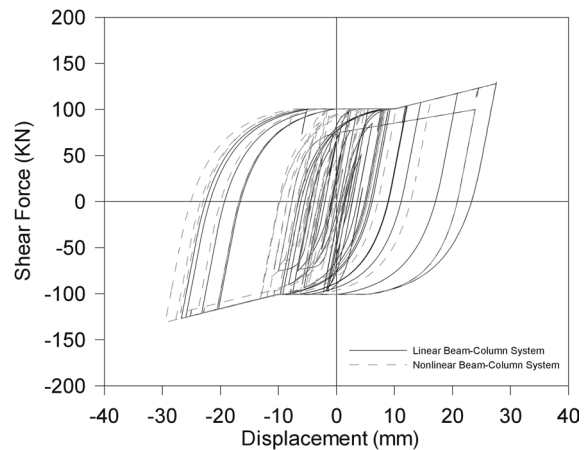


Fig. 17 Hysteresis loop of TPEA device at fifth story while structure is subjected to 0.9 g El Centro earthquake

beam-end for the structure equipped with TPEA devices and subjected to the El Centro earthquake of 0.9 g PGA is shown in Fig. 15. The moment-curvature relationship at the fifth story beam-end for the structure equipped with viscoelastic dampers and subjected to the El Centro earthquake of 0.8 g PGA is shown in Fig. 16. These figures imply that some parts of the members in the main structure have experienced inelastic deformations, and they can not to be detected by linear assumption of the main structure. The hysteresis loop of the TPEA device at the fifth story for the structure under the El Centro earthquake of 0.9 g PGA is shown in Fig. 17. The hysteresis loop of viscoelastic damper at the fifth story the structure under the El Centro earthquake of 0.8 g PGA is shown in Fig. 18. It could be found that once the behavior of the main structure is nonlinear, the seismic responses of passive devices with linear beam elements would be insufficient.

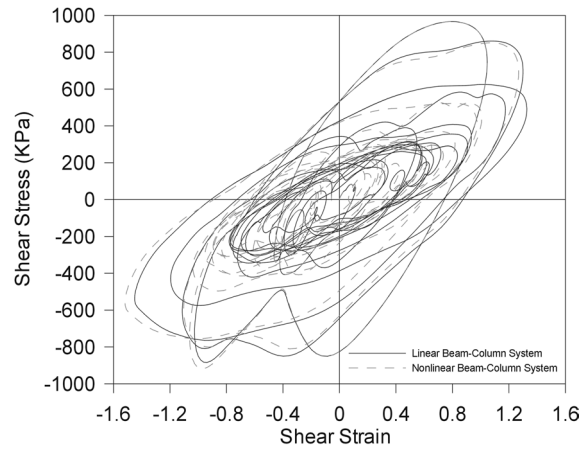


Fig. 18 Hysteresis loop of viscoelastic damper at fifth story while structure is subjected to 0.8 g El Centro earthquake

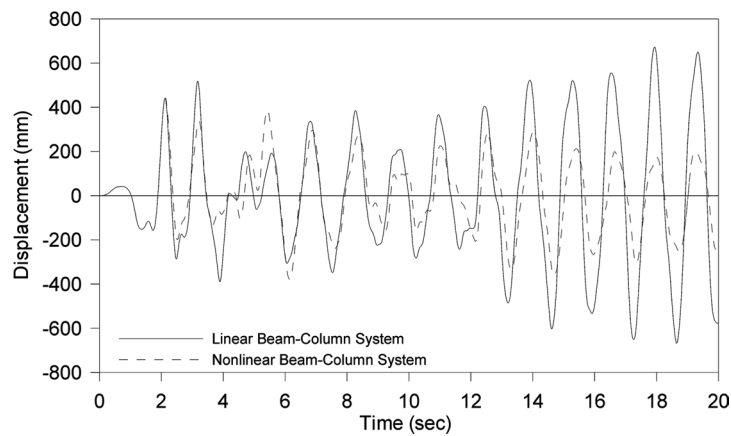


Fig. 19 Comparison of roof displacement while bare structure is subjected to 1.0 g El Centro earthquake

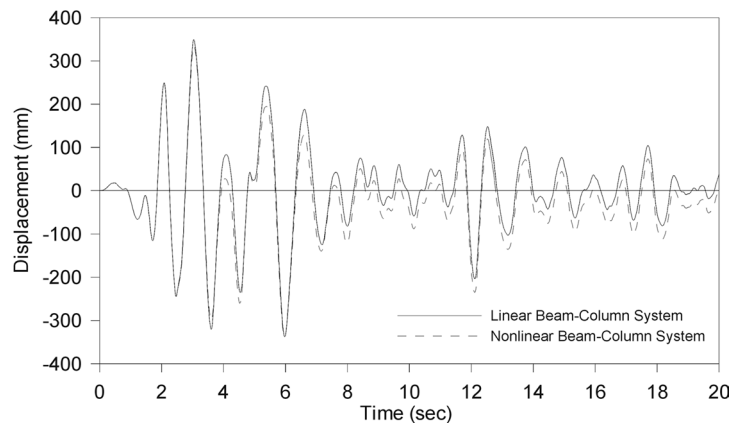


Fig. 20 Comparison of roof displacement for structure equipped with TPEA devices is subjected to 1.0 g El Centro earthquake

Figs. 19-21 present the comparisons of time-history responses of the roof displacement for the structure with and without dampers under the 1.0 g El Centro earthquake ground motions, respectively. These figures illustrate that simulated results are extremely different for various cases when the structure is subjected severe earthquake ground motions. The reason for this is that seismic energy is dissipated through yielding of the main structural members on the nonlinear beam-column system, and that the structural responses are improved a lot and much smaller than those for the linear beam-column system because of large amount of plastic hinges occurs on the beams of the main structure. The moment-curvature relationships at the fifth beam-end of the nonlinear beam-column systems with and without passive devices under the same earthquake excitation are shown in Figs. 22-24. It can be observed that during strong earthquakes, the bare structure without serious yielding of dampers may not be repaired after the strong earthquake

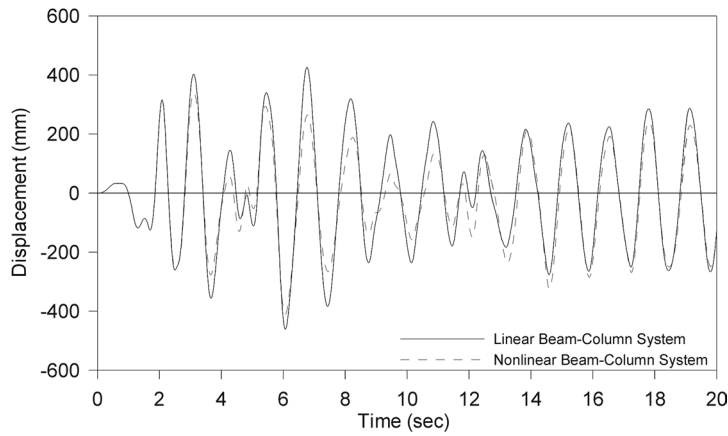


Fig. 21 Comparison of roof displacement for structure equipped with viscoelastic dampers is subjected to 1.0 g El Centro earthquake

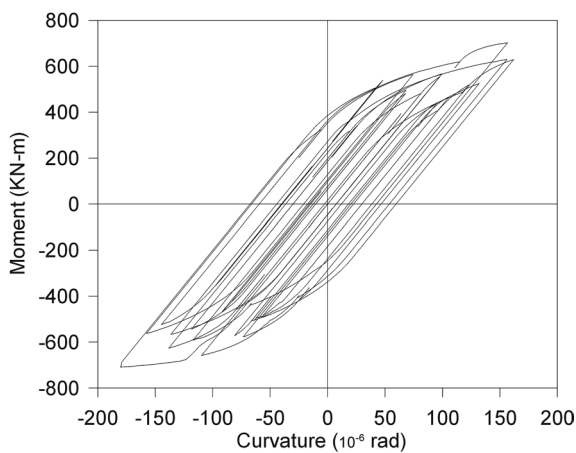


Fig. 22 Moment-curvature relationship at fifth story beam-end of bare frame under 1.0 g El Centro earthquake

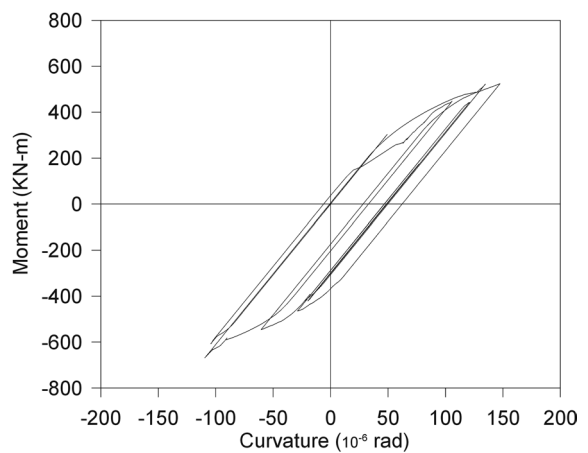


Fig. 23 Moment-curvature relationship at fifth story beam-end of structure equipped with TPEA devices under 1.0 g El Centro Earthquake

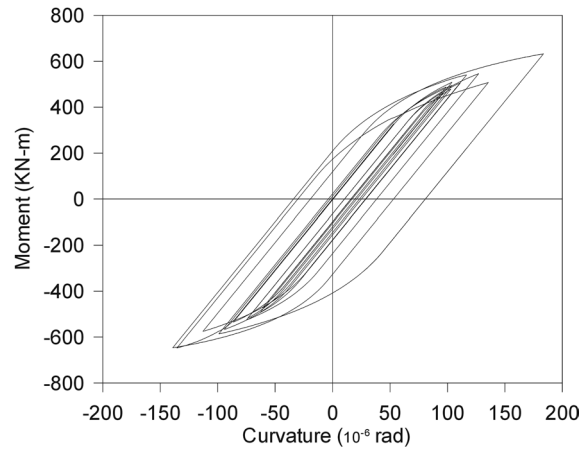


Fig. 24 Moment-curvature relationship at fifth story beam-end of structure equipped with viscoelastic dampers under 1.0 g El Centro earthquake

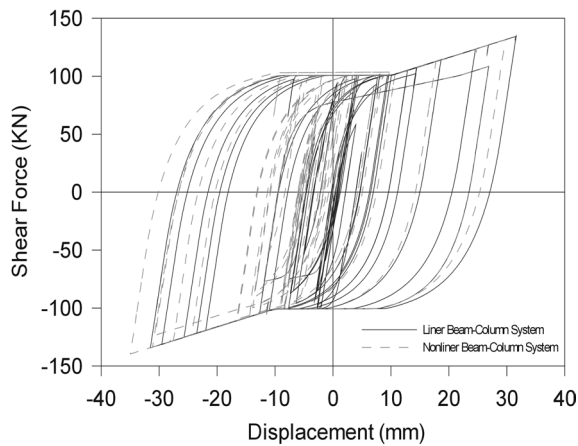


Fig. 25 Hysteresis loop of TPEA device at fifth story while structure is subjected to 1.0 g El Centro earthquake

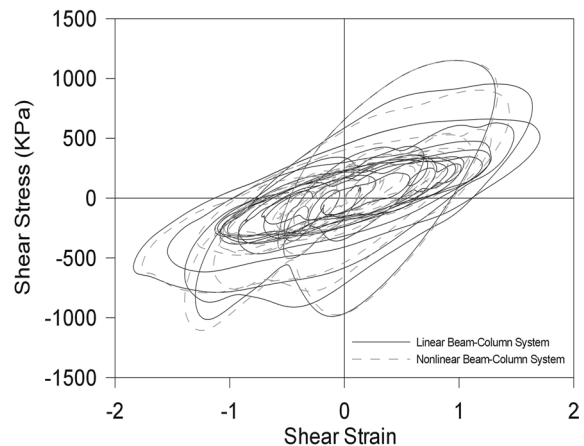


Fig. 26 Hysteresis loop of viscoelastic damper at fifth story while structure is subjected to 1.0 g El Centro earthquake

because of extremely large inelastic deformations. With the added passive devices, ductility demands on the members of the main structure can be substantially reduced. The hysteresis loops of the TPEA device and viscoelastic damper at the fifth story for the structure subjected to the 1.0 g El Centro earthquake are shown in Figs. 25 and 26, respectively. It can be seen that the simulated results of passive devices between the linear and nonlinear beam-column systems are obviously different. This indicates that the adoption of a linear beam-column system may not predict the responses of passive devices accurately when the realistic behavior of beams and columns is inelastic.

6. Conclusions

In order to analyze the responses of structures subjected to complex, nonproportional, and cyclic loadings, such as those resulting from strong ground motions, a precise nonlinear model is necessary. This paper presents a generalized plasticity model for predicting the behavior of structural members under the combinations of six components of applied forces, including the axial force, two transverse shear forces, two bending moments and the torsion. The nonlinear beam element formulated in this study can be applied to simulate the plastic hinge locations and extended areas and the damage of structures under strong seismic ground motions.

This study also presents one example of a structure with or without passive devices under different levels of earthquake ground motions. Numerical results reveal that the consideration of the nonlinearities in structural elements depends on the seismic intensities and the design hypothesis. The behavior of the example structure with or without passive devices is remained in linear range under minor earthquakes. Once earthquake intensity is larger, the adoption of nonlinear beam elements becomes necessary. Nonlinear analyses can also predict the damage style of a structure with or without passive devices, and the weak parts of the structural members can be strengthened in advance.

References

- Aiken, I.D., Kelly, J.M. and Pall, A.S. (1988), "Seismic response of a nine-story steel frame with friction damped cross-bracing", Report No. UCB/EERC-88/17, Earthq. Engng. Res. Ctr., Univ. of California at Berkeley, 1-7.
- Aiken, I.D., Kelly, J.M. and Mahmoodi, P. (1990), "The application of viscoelastic dampers to seismically resistant structures", *Proc. of 4th U.S. Nat. Conf. on Earthq. Engng.*, Palm Springs, California, **3**, 459-468.
- Bergman, D.M. and Hanson, R.D. (1990), "Viscoelastic versus steel plate mechanical damping devices: An experimental comparison", *Proc. of 4th U.S. Nat. Conf. on Earthq. Engng.*, Earthq. Engng. Res. Institute, Oakland, California, **3**, 469-477.
- Constantinou, M.C. and Symans, M.D. (1993), "Experimental study of seismic response of buildings with supplemental fluid dampers", *Struct. Design of Tall Buildings*, **2**(2), 93-132.
- Dafalias, Y.F. and Popov, E.P. (1975), "A model of nonlinearly hardening materials for complex loading", *Acta Mechanica*, **21**, 173-192.
- Kelly, J.M. and Skinner, M.S. (1980), "The design of steel energy-absorbing restrainers and their incorporation into nuclear power plants for enhanced safety (vol. 2): Development and testing of restraints for nuclear piping systems", Report No. UCB/EERC-80/21, Earthq. Engng. Res. Ctr., Univ. of California at Berkeley, California.
- Mahmoodi, P. (1972), "Structural dampers", *J. Struct. Div.*, ASCE, **95**(8), 1661-1672.
- Morz, Z. (1967), "On the description of anisotropic workhardening", *J. of Meth. Phys. Solids*, **15**, 163-175.
- Morz, Z. (1969), "An attempt to describe the behavior of metals under cyclic loads using a more general workhardening model", *Acta Mechanica*, **17**, 199-212.
- Pall, A.S., Ghorayeb, F. and Pall, R. (1991), "Friction dampers for rehabilitation of Ecole Polyvalente at Sorel, Quebec", *Proc. 6th Canadian Conf. On Earthq. Engng.*, Toronto, Canada, 389-396.
- Pekau, O.A. and Guimond, R. (1991), "Controlling seismic response of eccentric structures by friction dampers", *Earthq. Engng. Struct. Dyn.*, **20**(6), 505-521.
- Phillips, A. and Lee, C.W. (1979), "Yield surfaces and loading surfaces experiments and recommendations", *Int. J. Solids Struct.*, **15**, 715-729.
- Pong, W.S., Tsai, C.S. and Lee, G.C. (1994), "Seismic performance of high-rise building frames with added energy-absorbing devices", Tech. Rep. NCEER-94-0016, Nat. Ctr. for Earthquake Engrg. Res., State Univ. of New York at Buffalo.

- Prager, W. (1956), "A new method of analyzing stresses and strains in work-hardening plastic solids", *J. Appl. Mech.*, **23**, Trans., ASME, 493-496.
- Skinner, R.I., Kelly, J.M. and Heine, A.J. (1975), "Hysteretic dampers for earthquake-resistant structures", *Earthq. Engng. Struct. Dyn.*, **3**(3), 287-296.
- Steimer, S.F. and Chow, F.L. (1984), "Curved plate energy absorbers for earthquake resistant structures", *Proc. 8th World Conf. on Earthq. Engng.*, Earthq. Engng. Res. Institute, Oakland, California, **5**, 967-974.
- Tsai, C.S. (1993), "Innovative design of viscoelastic dampers for seismic mitigation", *Nuclear Engineering and Design*, **139**(2), 165-182.
- Tsai, C.S. (1994), "Temperature effect of viscoelastic dampers during earthquakes", *J. Struct. Eng.*, ASCE, **120**(2), 394-409.
- Tsai, C.S. (1996), *Nonlinear Stress Analysis Techniques*. -NSAT, Department of Civil Engineering, Feng Chia University, Taichung, Taiwan, R.O.C.
- Tsai, C.S. and Lee, H.H. (1993), "Applications of viscoelastic dampers to high-rise buildings", *J. Struct. Eng.*, ASCE, **119**(4), 1222-1233.
- Tsai, C.S. and Lee, H.H. (1994), Closure to "Applications of viscoelastic dampers to high-rise buildings", *J. Struct. Engng.*, ASCE, **120**(12), 3680-3687.
- Tsai, C.S. and Tsai, K.C. (1992), "ADAS devices for seismic mitigation of high-rise buildings", *Workshop on Base Isolation and Energy Dissipation Techniques for Structure*, Taipei, Taiwan, R.O.C.
- Tsai, C.S. and Tsai, K.C. (1995), "TPEA device as seismic damper for high-rise buildings", *J. Engng. Mech.*, ASCE, **121**(10), 1075-1081.
- Tsai, C.S., Chen, K.C. and Chen, C.S. (1998), "Nonlinear behavior of structures with added passive devices", *Proc. Second World Conf. on Structural Control*, Kyoto, Japan, **1**, 309-318.
- Tseng, N.T. and Lee, G.C. (1983), "Simple plasticity model of two-surface type", *J. Eng. Mech.*, **109**(3), 795-810.
- Whittaker, A., Bertero, V., Alonso, J. and Thompson, C. (1989), "Earthquake simulator testing of steel plate added damping and stiffness elements", Report No. UCB/EERC-89/02, Earthq. Engng. Res. Ctr., Univ. of California at Berkeley, California.
- Yang, C.F., Lee, E.T., Chang, K.C. and Lee, G.C. (1995), "Inelastic behavior of steel members under nonproportional loading", *J. Eng. Mech.*, **121**(1), 131-141.
- Zhang, R.H. and Soong, T.T. (1992), "Seismic design of viscoelastic dampers for structural applications", *J. Struct. Engng.*, **118**(5), 1375-1392.
- Ziegler, H. (1959), "A modification of Prager's hardening rule", *Quarterly Applied Mathematics*, **17**, 55-65.